Matching Generalized-Bicycle Codes to Neutral Atoms for Low-Overhead Fault-Tolerance

Joshua Viszlai^{1,*}, Willers Yang¹, Sophia Fuhui Lin¹, Junyu Liu¹, Natalia Nottingham¹, Jonathan M. Baker², Frederic T. Chong¹

¹University of Chicago

²University of Texas, Austin

Abstract—Despite the necessity of fault-tolerant quantum systems built on error correcting codes, many popular codes, such as the surface code, have prohibitively large overheads. This has spurred significant interest in quantum LDPC codes which can reduce this overhead by an order of magnitude. Unfortunately, this reduction comes at the cost of many long range interactions. The difficulty in implementing these long range interactions raises questions about the practical viability of quantum LDPC codes.

In this work we identify quantum LDPC codes that can be used in practice by carefully matching their features with underlying hardware. We target a specific family, known as generalized-bicycle codes, which have the favorable property of repeated check structure. We find this property can be exploited by quantum computers made from atom arrays, enabling an efficient implementation. Using numerical simulations, we evaluate the performance of generalized-bicycle codes in atom arrays and find comparable logical error rates to surface codes, but with an order of magnitude lower qubit overhead.

We then quantify the utility of this implementation in the context of a complete fault tolerant architecture. We compare the cost of implementing benchmark programs in a standard, surface code only architecture and a recently proposed mixed architecture where data is stored in qLDPC memory but is loaded to surface codes for computation. We treat the mixed architecture as a simple memory hierarchy and analyze the dependence of performance on program structure and compilation. Overall, for most programs of interest we find the mixed architecture leads to reduced costs compared to a standard, surface code only architecture. Additionally, we point out important compiler optimizations that emphasize qubit reuse and perform data prefetching to further improve the performance of the mixed architecture.

I. Introduction

In order to execute most quantum algorithms, we need orders of magnitude lower error rates than we can achieve physically. For example, chemistry and factoring algorithms can require error rates below 10^{-15} whereas reasonable expectations for physical error rates on many platforms are 10^{-3} [7]. To alleviate this gap between algorithmic requirements and physical capabilities, many researchers are focusing on developing **fault-tolerant** qubits. In a fault-tolerant quantum system, an application's quantum information is protected by underlying quantum error correcting (QEC) codes which encode the information over many physical qubits, allowing for continuous detection and correction of errors. This comes with a variety of challenges. The encoding process often

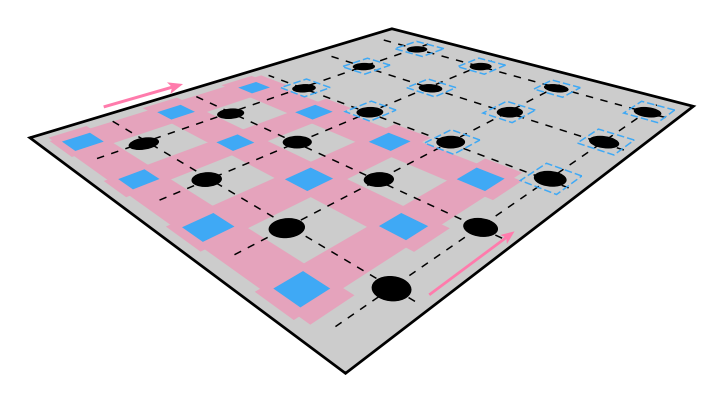


Fig. 1. A conceptual picture of this work: check qubits (squares) are moved together until they align with their respective data qubits (circles), allowing long-range operations to be performed in parallel. This is enabled by the repeated check structure inherent in the qLDPC codes we consider. The idea can then be implemented by a 2D AOD (pink lines) in atom array quantum computers.

introduces a large qubit overhead, and since all quantum devices have limiting physical error rates, information must *always* be encoded, including during logic operations. Additionally, parity checks require operations between ancilla qubits and data qubits, imposing connectivity requirements on the hardware. Overall, we can view a QEC code in terms of 1) its encoding capabilities: how efficiently it protects qubits, 2) it's logical capabilities: which qubit operations it can perform fault-tolerantly, and 3) it's hardware compatability: how efficiently the underlying checks can be implemented in a given hardware.

To date, no QEC code excels in all three of these areas. Popular codes such as the surface code only require nearest neighbor connections. This is compatible with superconducting hardware, but limiting checks to local operations is known to limit encoding rates [5]. Despite their poor encoding rates, surface codes still benefit from good logical capabilities, with techniques such as lattice surgery [22] enabling operations without additional hardware constraints.

Quantum low-density parity-check (qLDPC) codes have been a subject of great theoretical research recently and provide good encoding rates. Unfortunately this comes at the cost of non-local parity checks, limiting hardware compatibility. Furthermore, qLDPC codes often encode many qubits in a single block, creating difficulties for performing logic.

^{*}Correspondence: viszlai@uchicago.edu

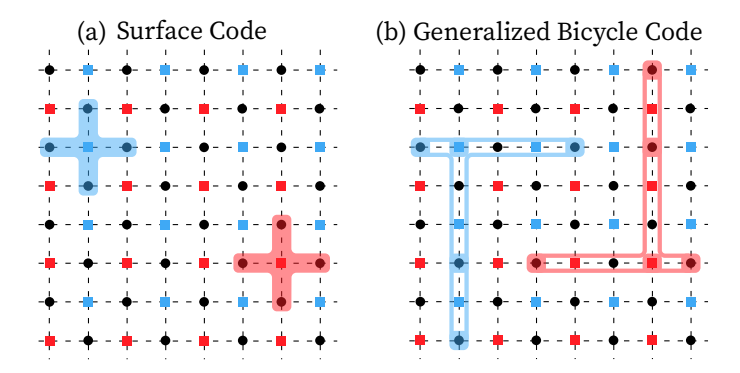


Fig. 2. Check structure, indicating the data qubits (circles) involved in each parity check (squares), for (a) a surface code and (b) an example of generalized bicycle codes. The structure is identical for all checks of the same type, with blue indicating X-type checks and red indicating Z-type checks.

Excitingly, recent research [10], [56], [59] has designed efficient implementations of certain qLDPC codes for hardware made from superconducting qubits and atom arrays, improving their hardware compatibility. In this work, we also take a step in this direction by addressing a family of qLDPC codes known as generalized-bicycle codes [24]. Compared to the surface code in Figure 2, generalized-bicycle codes preserve a repeated check structure but introduce non-local checks. We show how this is good fit for atom array devices which can efficiently implement many of these non-local checks in parallel through the use of mid-circuit movement.

In addition to addressing the hardware compatibility of generalized-bicycle codes, we also quantify their utility in a full fault-tolerant architecture that includes logical operations. Using a recently proposed model we analyze an architecture with three types of QEC systems. 1) Generalized-bicycle codes that serve as efficient quantum memory, leveraging their good encoding capabilities 2) A small number of surface codes that perform computation, leveraging their good logical capabilities, and 3) Ancilla systems that teleport data between qLDPC memory and surface code compute, which can be implemented in atom arrays [59]. Treating this mixed code architecture as a simple memory hierarchy, we evaluate a suite of benchmark programs and compare with a surface code only architecture. Overall we find that for most programs of interest the spatial savings of generalized-bicycle codes outweighs the temporal overhead of loading and storing data between memory and compute. We also point out compiler optimizations that further improve performance on the mixed architecture by prefetching qubits and emphasizing qubit reuse.

II. BACKGROUND

For background on quantum computing fundamentals we refer to [15], [35], [43]. In this paper we give relevant background on quantum error correction and atom array quantum computers.

A. Quantum Error Correction

In this subsection we aim to give intuitive background information on quantum error correction (QEC) to aid in

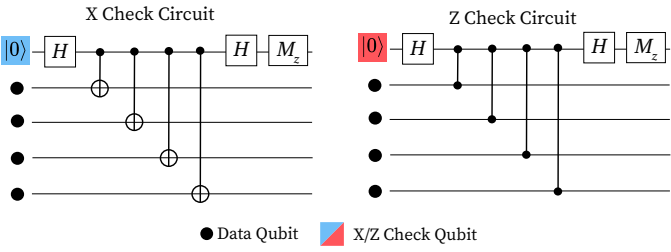


Fig. 3. Circuits for performing an X parity check and a Z parity check.

understanding the key concepts of this work. However, for a more formal and in-depth background on QEC theory and concepts we refer to [18], [44].

The purpose of quantum error correction (QEC) is to translate our faulty physical device into a high-fidelity logical system. Using QEC codes, groups of physical qubits create encoded logical qubits with exponentially lower error rates. This encoding process requires performing parity checks between physical qubits to detect and correct errors, as specified by the given QEC code. In this work we only consider codes where parity checks are either X-type, checking only phase errors, or Z-type, checking only bit errors. Codes satisfying this property are called CSS codes [12]. Physically, parity checks can be mediated by an ancillary check qubit, also known as a syndrome qubit or ancilla qubit. Figure 3 shows the circuit structure for performing the two types of parity checks where the result is the check qubit's measurement output. Notably, the circuit requires gates between the check qubit and the data qubits being checked, imposing connectivity constraints at the hardware level. Additionally, these physical circuits are also error-prone and allow errors to propagate between qubits via the two qubit gates. The number of data qubits involved in a check is called the weight, and codes with higher weight checks can suffer from more error propagation.

A given QEC code specifies a number of physical qubits, n, and a set of parity checks, also called stabilizers. The shared eigenspace of the stabilizers forms the error-protected space for the encoded qubits. The number of encoded logical qubits is k and the level of error protection can be captured by the code distance, d, which is the number of physical qubit errors required to create a logical qubit error. Overall, QEC codes are commonly described using these three numbers, [n, k, d].

In order to correct errors, the results of parity checks also need to be decoded, inferring the most likely physical errors. These entails a decoding algorithm running on classical hardware. Since decoding must happen in real-time, the classical processing is limited by the coherence of the quantum device. This can put significant strain on fast devices, such as superconducting qubits. If check data is generated faster than can be decoded, a backlog occurs which exponentially slows down computation [54]. As a result, a requirement for QEC in practice is the ability to perform real-time decoding [50], [53], [58].

In addition to encoding logical qubits, our logical system also needs to support error-protected gates on logical qubits. A

common set of gates that can be implemented fault-tolerantly is the Clifford group: $\{X, Y, Z, S, H, \text{CNOT}\}$. This is not a universal gate set, however, and so a common additional gate that is used is the T gate. The T gate requires more involved techniques to reach requisite logical error rates, however, such as magic state distillation [11], [29].

B. Atom Arrays

Atom arrays are quantum computers made from a 2D arrangement of optically trapped atoms [4], [8], [23], [33]. These devices have long coherence times on the order of seconds [4], [23], [33], high-fidelity gates [17], and allow for mid-circuit movement of atoms [8]. The later is enabled through the use of 2D Acousto-Optic Deflectors (AODs), which control movement in the X and Y directions. This allows for 2D movement of a grid of atoms as well as stretching and squeezing, so long as the trapping lasers do not cross.

Multi-qubit gates in these devices are mediated by the Rydberg interaction. The $|1\rangle$ state is coupled to a highly-excited Rydberg state, which blockades the same transition on neighboring atoms via van der Waals forces. The resulting interaction creates a CZ gate between atoms. By moving atoms that need to interact near each other, a global pulse can be used to execute many CZ gates in parallel [17]. Furthermore, the strength of the Rydberg interaction scales $\propto \frac{1}{r^6}$ where r is the distance from the excited atom. This means cross-talk can be removed by spacing non-interacting atoms sufficiently far apart.

III. RELATED WORK

In a recent paper, Xu et al. [59] also proposed an implementation of qLDPC codes on atom arrays. They implement parity check circuits via 1D atom rearrangements that are applied to rows and columns of an atom array, matching the product structure of the codes they consider with the product structure of AODs. In our work the atoms that serve as check qubits are instead moved collectively in 2D, leveraging the repeated check structure of the codes we consider. We also address smaller blocks of qLDPC codes that may be more feasible for near-term implementation. There has also been prior work on implementing other types of QEC codes, such as surface code [1], [57], on atom arrays. Compiling NISQ algorithms for atom arrays has also been a subject of research [3], [31], [36], [38], [39], [51], [52], however many of these techniques would require adaptation to apply in a fault-tolerant setting.

Some prior works explored how qLDPC codes can be implemented on other types of hardware. Notably, IBM's recent work [10] showed that the Tanner graphs of some quasi-cyclic qLDPC codes can be partitioned into two planar subgraphs. As a consequence, the codes can be realized on a planar superconducting chip with long range links. Previously, Tremblay et al. [56] proposed to implement qLDPC codes on a small number of planar layers, such that each layer contains long-range connections which do not cross. Pattison et al. [40] proposed to use a concatenation of surface code and qLDPC

codes, which reduces the hardware connectivity requirement to the nearest-neighbor connectivity of surface code at the expense of lowering the encoding rate. Some works [13], [42], [60] proposed methods to implement logical gates on qLDPC codes, however, hardware implementations of these methods have not be discovered in general.

IV. GENERALIZED BICYCLE CODES

In this section we give a brief explanation of the code construction we use throughout the paper. The construction we use is not novel, but we include it for completeness and to improve clarity. That said, the main discussion of its use in Section V should still be accessible without fully understanding the construction.

A. Code Construction

The qLDPC codes we address in this work are instances of generalized bicycle codes [24]. To start, we consider the $l \times l$ cyclic shift matrix S_l . If we view rows as parity checks and columns as data qubits, S_l maps check i to data qubit i+1 mod l. More generally, any power S_l^p maps check i to data qubit $i+p \mod l$. In total this gives l unique matrices. For example with l=3:

$$S_3 = \begin{bmatrix} 0 & 1 & 0 \\ 0 & 0 & 1 \\ 1 & 0 & 0 \end{bmatrix} S_3^2 = \begin{bmatrix} 0 & 0 & 1 \\ 1 & 0 & 0 \\ 0 & 1 & 0 \end{bmatrix} S_3^3 = I = \begin{bmatrix} 1 & 0 & 0 \\ 0 & 1 & 0 \\ 0 & 0 & 1 \end{bmatrix}$$

This gives a convenient mapping to an algebra where terms x^p represent cyclic matrices S_l^p . Extending this to two variables, x, y, we use terms defined as

$$x^p y^q = S_l^p \otimes S_m^q \tag{1}$$

with p < l, q < m. We can then construct matrices from polynomials over x, y

$$A = a(x, y), B = b(x, y) \tag{2}$$

Finally, the generalized bicycle code is specified via check matrices

$$G_x = (A|B), G_z = (B^T|A^T)$$
 (3)

A specific instance of the code is identified by parameters l,m and polynomials a,b. For example, a [128, 16, 8] code is derived from l=8,m=8 and polynomials

$$a(x,y) = y + y^{2} + y^{5} + x^{6}$$
$$b(x,y) = y^{2} + x^{2} + x^{3} + x^{7}$$

If we set m=1, this construction reduces to polynomials over the single variable x and we recover the definition provided in [24]. Constraining a, b to be trinomials with terms consisting of only x^p or y^q , we get the quasi-cyclic codes introduced in [10]. The construction we use can also be viewed as a two-block group algebra code where the group is a cyclic group [27].

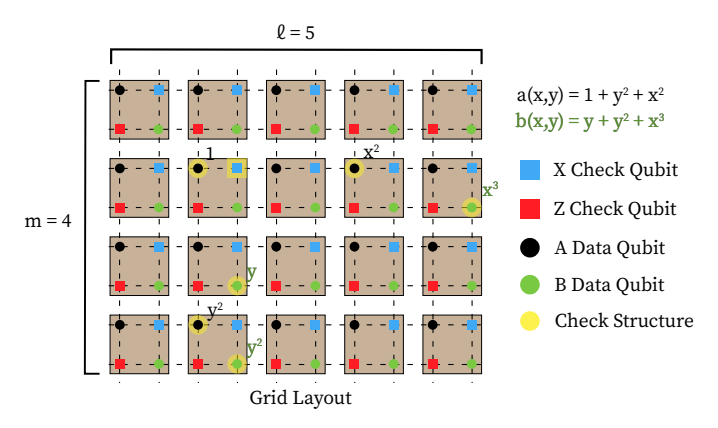


Fig. 4. The qubit layout we use for generalized-bicycle codes. This specific example corresponds to a code with l=5, m=4 and polynomials $a(x,y)=1+y^2+x^2$, $b(x,y)=y+y^2+x^3$, which describe the data qubits involved in each parity check. Each subgrid (X check, Z check, A data, B data) is mapped identically and interleaved. The highlighted check structure shows the relative position of data qubits from a given X check qubit. This structure is identical for all X check qubits up to periodic boundary conditions. Z check qubits have a mirrored structure.

B. Qubit Layout

We first highlight the structure of the check matrices. As an example, take $A=1+y^2+x^2$ for l=5, m=4:

$$A = \begin{bmatrix} I + S_4^2 & 0 & I & 0 & 0 \\ 0 & I + S_4^2 & 0 & I & 0 \\ 0 & 0 & I + S_4^2 & 0 & I \\ I & 0 & 0 & I + S_4^2 & 0 \\ 0 & I & 0 & 0 & I + S_4^2 \end{bmatrix}$$

A is a $lm \times lm = 20 \times 20$ matrix where each row has three non-zero entries. A natural mapping procedure maps each block of m qubits to a column on the device. Performing this mapping for both data and checks, we get two $m \times l$ grids. We identify check/data qubit i with the i^{th} row/column in our matrix A. The qubit is then mapped to the device at position $(row, col) = (i \mod m, \lfloor i/m \rfloor)$ in the check/data qubit grid.

To map the whole code, we can use this procedure for all qubits. Namely, from our X and Z check matrices in Equation 3, we have four groups of qubits: X checks, Z checks, data in A, and data in B. This gives four $m \times l$ grids which can be interleaved, as shown in Figure 4.

C. Parity Check Structure

An identifying property of generalized-bicycle codes that is important to this work is the repeated check structure. Each term $x^p y^q$ defines a check operation mapping each check to a data qubit with the relative position between the two being identical for all X(Z) checks, up to periodic boundary conditions.

Handling Periodic Boundary Conditions

Given a term $x^p y^q$, the mapping from check qubit to data qubit might go beyond the boundaries. Since boundaries are periodic, this changes the relative position. To address this, we can derive all possible relative positions between check and data qubits in our mapping. With no periodicity, the relative

position between check i and its data qubit is (row, col) = (q, p). If $i \ge m(l-p)$, we have horizontal periodicity and the column offset is changed to (p-l). If $i \mod m \ge (m-q)$, we have vertical periodicity and the row offset is changed to (q-m). Overall, this gives four possible relative positions: (q, p), (q, p-l), (q-m, p), (q-m, p-l). Additionally, if p=0 or q=0, this reduces to only two possibilities.

V. EFFICIENT QUANTUM MEMORY IN ATOM ARRAYS

In this section we discuss how generalized-bicycle codes can be efficiently implemented on atom array quantum computers, motivating the feasibility of qLDPC for reducing the overhead of fault-tolerance in practice.

A. Code Selection

As a family of qLDPC codes, generalized-bicycle codes have promising asymptotic encoding rates and recent work has additionally found many instances of generalized-bicycle codes with good encoding rates, even at small sizes [10]. This makes them attractive even in the near term compared to more standard QEC codes, such as the surface code, that suffer from poor encoding rates. For example, encoding 12 logical qubits at distance 11 requires 1452 data qubits with the surface code, but only 144 data qubits with a generalized-bicycle code. This substantially better encoding rate does not come without additional challenges, however. Figure 2 shows a comparison between the types of parity checks in a surface code versus in a generalized-bicycle code. At the hardware level, the surface code only requires nearest neighbor interactions. On the other hand, the generalized bicyle code, like many qLDPC codes, requires many non-local interactions which can be difficult for most hardware platforms. An identifying feature, however, of generalized-bicycle codes is that the check structure, although non-local, is repeated. The relative position of a check qubit to its respective data qubits can be made identical for all check qubits, up to periodic boundary conditions. This is a great match for the atom array platform, where a 2D AOD can move grids of atoms in parallel. Furthermore, global pulses can induce local entangling operations on neighboring atoms, enabling the two qubit gates required between check qubits and data qubits. Using these hardware features, we describe how generalized-bicycle codes can be efficiently implemented in atom array systems

B. Implementing Parity Checks

At the circuit level, our goal is to implement the circuits of Figure 3 for all X and Z checks in our code. Since single qubit rotations can be performed with high fidelity in atom arrays [25], we focus on describing how the long-range two qubit gates between check and data qubits are performed.

We separate the logical cycle into two halves, corresponding to X checks and Z checks, each broken into w steps, where w is the weight of our parity checks. For each step we implement one term x^py^q from our parity check structure. This ensures the relative position between an X(Z) check qubit and its data qubit in that step can be made identical for all X(Z) checks, up

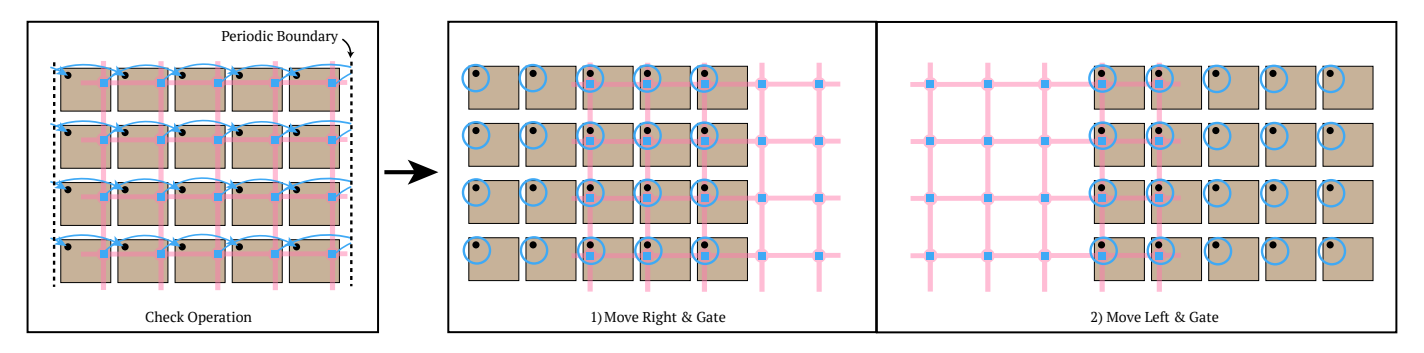


Fig. 5. Implementation of a single check operation, x^2 , for all X checks in a small example code. Check qubits are moved together using a 2D AOD (pink lines) and the relative position from check qubit to data qubit is (row, col) = (+0, +2). Due to periodic boundary conditions, a subset of checks have horizontal periodicity, resulting in a relative position of (+0, -3). Overall this requires two global pulses, one for each relative position.

to periodic boundary conditions. Using an AOD we can move all X(Z) checks over by this relative position, aligning each X(Z) check qubit with its respective data qubit. A global pulse is then applied to perform the two qubit gate between each check qubit and its now adjacent data qubit. Due to periodic boundary conditions, however, a subset of check qubits near the boundary will go beyond the code block. These qubits have a separate relative position, as described in Section IV-C, and require a second movement operation and global pulse. For all but one of the codes we simulate, each step only requires two global pulses, and in the worst case the code construction we consider can require four global pulses each step.

Figure 5 gives an example of implementing a check operation for all X checks in a small code. In the circuit picture of Figure 3 this can be viewed as performing one CNOT gate for all X checks. To implement a full code cycle, we repeat this for all X check operations and for all Z check operations. At the circuit level, this is equivalent to the coloration circuit described in [56], where each check operation x^py^q is a color. Although notably the time taken for movement allow additional idle errors to occur. We make sure to model these idle errors in our simulations described in Section VI.

C. Hardware Compatibility

A key hardware feature required for our implementation is the collective movement of 2D grids of check qubits. In atom arrays, coherent movement of a 2D array of qubits via an AOD has been experimentally demonstrated in the context of quantum error correction [8], [59]. Additionally, movement speeds of 0.55 $\mu m/\mu s$ have been demonstrated with atom separations of 5-10 μm . This has lead to movement times for the surface and hypergraph product codes of \sim 1-10 ms. Via simulations described in Section VI, a single round of the generalized-bicycle codes we consider requires a similar amount of movement: ~5-10 ms. Although longer than typical gate times which occur on the order of μ s, this is still less than reported coherence times on the order of seconds [4], [23], [33]. High-fidelity parallel CZ gates on adjacent qubits and single-qubit rotations have also been demonstrated experimentally with error rates of $\sim 5 \times 10^{-3}$ and $< 10^{-3}$, respectively [17], [25], [34]. Most notably, these error rates are below the threshold for many QEC codes, including the surface code and the generalized-bicycle codes we consider. Various methodologies for mid-circuit measurement also exist in experiment [8], [21], [48], [49], however, current measurement error rates are $\sim 5\times 10^{-2}$, which is just above the threshold for most codes. A notable contributor to measurement errors that's important to mention is atom loss. This has been a topic of much recent research, with promising directions for improvement. For example, [34] mentions that future non-destructive measurement techniques can be used to detect and correct atom loss events during measurement.

Concerning the scalability needed for QEC, machines with > 250 atoms exist in experiment [16], [49] which is more qubits than is needed for many of the generalized bicycle codes we consider.

VI. SIMULATING CODE PERFORMANCE

We evaluate the performance of our proposed implementation via numerical simulations. We construct generalized-bicycle codes from code parameters l, m, a(x, y), b(x, y) as described in Section IV and compile their parity check circuits into a Stim [20] circuit.

A. Error Modeling

In our simulations we use a full circuit-level noise model for a physical error rate p that includes propagation of errors during the parity check circuits. Single qubit gates are followed by $\{X,Y,Z\}$ errors with probabilities $\frac{p}{3}$. Two qubit gates are followed by $\{I,X,Y,Z\} \otimes \{I,X,Y,Z\} \setminus II$ errors with probabilities $\frac{p}{15}$. Qubit reset and measurement are flipped with probability p.

In our compilation process we also model the underlying movement operations. Idle errors are added after each movement operation using pauli twirling approximations [19]. The movement time is estimated using the same assumptions as prior work [59]. Moving distance l takes time $\sqrt{6l/a_p}$ where we assume the acceleration a_p is $0.02\mu m/\mu s^2$ and the spacing between atoms is $5\mu m$.

B. Decoding

We find that for memory, the generalized bicycle codes we simulate can be decoded using single shot decoding [9].

Including initialization, our simulations decode over two parity check cycles instead of over d+1 parity check cycles. For decoding, we use the BP-OSD decoder [37] available in the ldpc python package [45], [46]. The decoding hyperparameters we use are a maximum number of iterations of 10,000, the min-sum BP method, and the combination-sweep OSD with order 10. As is standard for CSS codes, we separate circuit-level decoding into X and Z sub-problems, each only decoding errors that flip X or Z checks, respectively. For the codes we simulate, we find one round of decoding takes ~ 1 ms. This is faster than the overall circuit which varies from 5-10 ms due to movement. This means that if data transfer times to/from the decoder are < 4 ms, the BP-OSD decoder could be used for real-time decoding of the codes we simulate.

C. Code Selection

To evaluate the performance of our proposed implementation we select a handful of generalized bicycle codes. Finding good codes in practice is non-trivial, as many choices of l, m, a(x, y), b(x, y) yield poor codes. Instead, we leverage recent works on qLDPC codes that provide many good codes that can be described as generalized-bicycle codes. We first choose three codes from recent work on quasi-cyclic codes [10]. These can be seen as instances of generalizedbicycle codes with trinomials a(x, y) and b(x, y) where terms are only either x^p or y^q . We also look at recent work on twoblock group algebra codes [27]. In this context the generalizedbicycle codes we address are a limiting case when the group being considered is a cyclic group. The set of codes we simulate are shown in Table I. # Steps/Op indicates the number of movements and global pulses necessary for each check operation as described in Section IV-C. Mixed x, y terms require 4 steps due to the presence of both horizontal and vertical periodicity. All other terms require 2 steps.

We select codes to evaluate the impact of check weight in our implementation. We choose three codes of weight 6 and three codes of weight 8. We also found a weight 8 code ([128,16,8]) with similar structure to the weight 6 codes for this purpose. We also evaluated a code with a 1D layout ([72,8,10]) and a code with terms requiring 4 steps per operation ([96,10,12]). These codes have higher movement requirements which increase idle errors.

D. Results

Figure 6 shows the results of our circuit-level simulations. The logical observables for each encoded qubit were found using the same methodology described in Section 8.1 of [10]. The left plot varies the parameter p in our error modeling described in Section VI-A with coherence times set to 10 seconds. In the right plot p is set to 10^{-3} and the coherence time is varied. We simulate generalized-bicycle codes for a single round and we simulate the surface code for d=12 rounds. For each data point we collected N_s shots and define N_e as the number of shots where a logical error occurred, N_s was chosen dynamically until at least 1,000 errors occurred, or 10^9 shots occurred. All data points accumulated at least 200

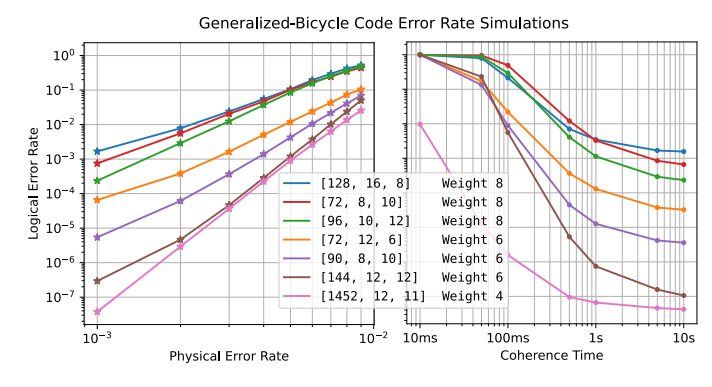


Fig. 6. Logical error rate simulations of the generalized-bicycle codes in Table I using our proposed atom array implementation. The simulations also include a surface code plot for comparison, generated from simulating 12 surface codes ([1452, 12, 11]).

errors. The plotted logical error rate p_L is then defined per round. For the generalized-bicycle codes this is $p_L = N_e/N_s$. For the surface code d=12 rounds occur and so we calculate $p_L = 1 - (1-(N_e/N_s))^{1/12} \approx \frac{(N_e/N_s)}{12}$.

Our results indicate that our implementation of the weight 6 generalized-bicycle codes has a comparable logical error rate to surface codes but with a significantly better encoding rate. We also find the weight 8 codes have poorer performance. This can likely be attributed to the longer circuits necessary for the higher weight checks leading to increased error propagation. We note, however, that we do not search over all possible circuits that implement the weight 8 codes and different circuits may have more robustness to error propagation. We see our results as a tentative confirmation of the effects of error propagation in higher weight codes, but believe a more thorough analysis should be performed in future work. Our coherence sensitivity results also show that the generalizedbicycle codes are more sensitive to coherence times than the surface code, as expected. However, the generalized-bicycle codes are still feasible since coherence times in experiment are on the order of seconds [4], [23], [33].

VII. EFFICIENT MEMORY IN A FAULT-TOLERANT ARCHITECTURE

In this section, we evaluate the utility of generalizedbicycle codes in a complete fault-tolerant system. Although we evaluate generalized-bicycle codes, much of the results we find are applicable to qLDPC codes in general.

A concern when considering qLDPC codes, including generalized-bicycle codes, is the relative difficulty of performing logical operations. Operations can be done in theory [13], but in general it is unknown how to embed the necessary ancilla systems in hardware. This is in contrast to the surface code which can implement operations via lattice surgery without increasing hardware connectivity costs [22]. In light of this, recent work on qLDPC codes in atom arrays has also shown how to implement an ancillary system that can teleport data between a qLDPC block and a surface code [59]. Computation can then be done on a small number of surface

[n,k,d]	l, m	a(x,y)	b(x,y)	Check Weight	# Steps/Op	Source				
[72, 12, 6]	6,6	$y + y^2 + x^3$	$y^3 + x + x^2$	6	2	[10]				
[90, 8, 10]	15, 3	$y + y^2 + x^9$	$1 + x^2 + x^7$	6	2	[10]				
[144, 12, 12]	12, 6	$y + y^2 + x^3$	$y^3 + x + x^2$	6	2	[10]				
[128, 16, 8]	8,8	$y + y^2 + y^5 + x^6$	$y^2 + x^2 + x^3 + x^7$	8	2	This work				
[72, 8, 10]	36, 1	$1 + x^9 + x^{28} + x^{31}$	$1 + x + x^{21} + x^{34}$	8	2	[27]				
[96, 10, 12]	12, 4	$1 + y + xy + x^9$	$1 + x^2 + x^7 + x^9y^2$	8	2 or 4	[27]				
TABLE I										

SELECTED CODES USED IN NUMERICAL SIMULATIONS

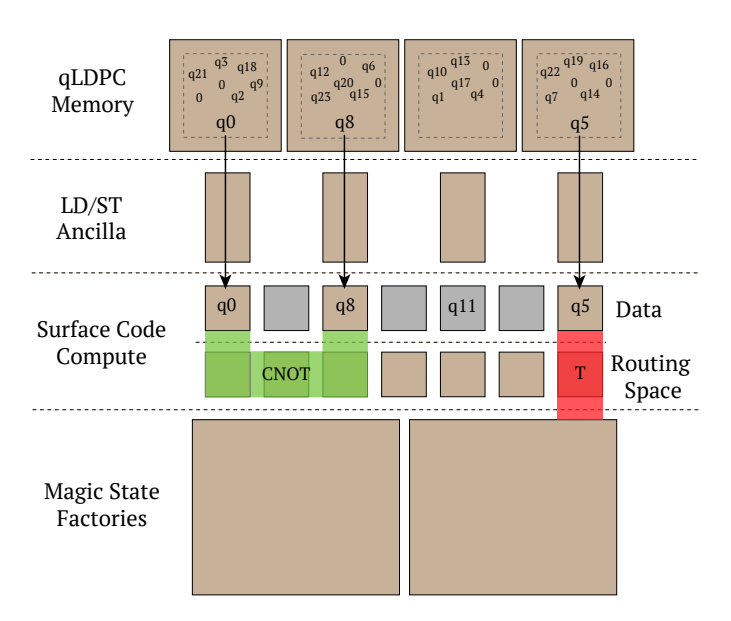


Fig. 7. A planar layout of the mixed qLDPC+surface code architecture discussed in Section VII

codes. This limits the additional hardware complexity. The only new ancilla system needed is one that can teleport qubits between qLDPC codes and surface codes.

In this architecture, shown in Figure 7, qLDPC codes are used as efficient memory systems, surface codes are used for computation, and data transfer between the two is enabled by teleportation systems. We claim the use of generalizedbicycle codes is beneficial if the overall cost is cheaper in this mixed architecture than in a surface code only architecture. In our evaluation we define cost as spacetime volume. The reason being if instead we define cost solely in terms of space, then the mixed architecture is trivially cheaper. By allocating the minimum number of surface codes possible we minimize the overall qubit footprint. Unfortunately, this serializes any program, potentially inserting large amounts of load and store operations, increasing the cost in time. Similarly, if we instead define cost solely in terms of time, then the surface code only architecture is trivially cheaper. By having our data always available for computation, we never have to insert load and store operations; however, in doing so, we suffer from the surface code's poor encoding rate, increasing the cost in space. Instead of using either extreme, a reasonable metric is therefore their product-the spacetime volume. Furthermore, given a model where quantum

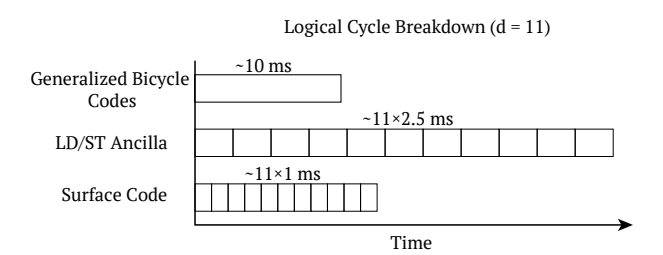


Fig. 8. The breakdown of a distance 11 logical cycle for the three code types necessary for a mixed qLDPC surface code architecture. Each segment indicates a round of parity checks.

Gate	# Logical Cycles	Code Type					
X, Y, Z, H, S	0	-					
CNOT	2	Surface Code					
T	2	Surface Code					
Load	2	LD/ST Ancilla					
Store	1	LD/ST Ancilla					
TABLE II							
GATE COSTS USED IN ESTIMATES							

computers are a shared resource, the spacetime volume is a useful economic metric to minimize.

Based on spacetime volume, the relative cost of the two architectures is dependent on the program being run. To better understand the dependency on program structure, we evaluate various benchmark circuits and analyze the impact of compiler performance on the resulting spacetime volume.

A. Evaluation Parameters

We perform our evaluation based on atom array quantum computers. We assume qLDPC memory is made of generalized-bicycle codes and we use costs from our results in Section VI. We assume the load/store ancilla is constructed according to [13] to implement a ZZ measurement between a qLDPC qubit and a surface code qubit. This can be treated as a hypergraph product code and implemented in atom arrays according to [59], with a space cost of $\sim 2d^2$ qubits. This allows for the use of the circuit in Figure 3 of [41]. Since the temporal cost of loads and stores is high we find this ancilla system best minimizes the overall spacetime volume by requiring only a single ZZ operation. Finally, we assume the surface codes can be implemented in atom arrays using the methodology from [8]. We assume the surface codes use the wide design from [30] and cost $2d^2$ qubits each, allowing single-qubit Clifford gates to be done in software.

Table II shows the number of logical cycles we assume each operation takes to execute. CNOT requires a ZZ measurement followed by a XX measurement which takes 2 logical cycles when implemented using lattice surgery [22], [28]. T gates are performed via state injection, consuming a T state produced in a magic state factory. This requires a CNOT gate and so we count the gate cost as 2 logical cycles. Load and Store both only require a ZZ measurement between a qLDPC and surface code qubit, which takes 1 logical cycle. This is followed by measuring out the old qubit location. For Store this is the surface code, and can be done in a single measurement. For Load this is a qubit in qLDPC memory. To avoid disturbing the other qubits in the memory block, we must re-use the qubits in the LD/ST ancilla system to measure out the gLDPC qubit using a system according to [13]. Like the LD/ST system, this can also be treated as a hypergraph product code and implemented in atom arrays according to [59]. In total, this means Load takes two logical cycles, one for measuring ZZand one for measuring out the old qLDPC qubit.

Figure 8 gives an overview of the temporal cost of a logical cycle in each code type. We find the time for generalized bicycle codes from our simulations. The time for the LD/ST ancilla is estimated using Equation 7 of [59] and the surface code time comes from [8]. We use these along with the gate costs of Table II to estimate program costs.

We also make two simplifying assumptions. First, we assume that each LD/ST ancilla can only operate on one qubit, meaning two logical qubits can't be loaded or stored from the same memory block simultaneously. Second, to account for the cost of T state distillation, we assume that all T states are generated via 15-to-1 magic state factories [11], implemented in surface codes as described in [29].

B. Mixed Architecture Layout

Figure 7 shows the layout we consider for the mixed qLDPC+surface code architecture. We assume all memory blocks are implemented with the same generalized-bicycle code. This adds a couple hardware features. First, since they all use the same code the same AOD can be used to move the check qubits in all blocks in parallel. Second, our implementation moves check qubits beyond the boundaries, as shown in Figure 5. This requires buffer space between memory blocks. Notably, if memory blocks are moved together, the buffer space between adjacent blocks can be shared. We can also leverage the ability of AODs to squeeze portions of the 2D grid being moved to consolidate check qubits beyond the boundary [8]. If CZ pulses can be focused within memory blocks, the consolidation can be significant, otherwise the spacings need to be large enough to avoid unwanted Rydberg interactions. In either case however, the total space is still substantially less than the space required for the same number of qubits in the surface code. With no squeezing and spacings of $5\mu m$, 48 qubits in four qLDPC memory blocks using the [144,12,12] generalized-bicycle code has a total footprint of $0.06 \ mm^2$. The same 48 qubits in 48 d=11 surface codes would have a total footprint of $0.58 \ mm^2$.

LD/ST ancilla systems are laid out to connect memory blocks to a subset of the surface codes. We assume the use of an AOD allows for the LD/ST ancilla to selectively connect one of potentially many surface codes to the memory block. In the example of Figure 7, each LD/ST ancilla is assigned 1 memory block and 2 surface codes, except for the right-most which is assigned 1 surface code.

The surface code compute section consists of a row of surface codes which house data, and a row of surface codes for routing CNOT and T gates via lattice surgery. This is also the same layout used in the baseline surface code only architecture.

In the layout we consider, a section of the device is dedicated to producing magic states in magic state factories. The underlying code is also surface codes, and we assume these surface codes connect to the routing space, allowing for T state injection.

C. Compilation Methodology

For compilation, we operate on input programs that have already been synthesized into a fault-tolerant gate set of Clifford + T using standard approaches [35], [47]. The main task of compilation is therefore to: 1) map qubits to qLDPC memory blocks, 2) insert load and store operations, and 3) route gates in the surface code.

Mapping Qubits: A slowdown that can be attributed to poor mapping occurs when a CNOT operates on two qubits in the same memory block. Since two qubits cannot be loaded from the same memory block simultaneously, their loads must be serialized. A reasonable heuristic therefore is to maximize the number of number CNOT gates with qubits mapped to different memory blocks. For a program with Q qubits, we formulate this as an integer programming problem and solve with IBM's CPLEX:

$$\max\sum_{n=1}^N w_{i,j} \text{CNOT}_{i,j}$$
 s.t.
$$\sum_{n=1}^N q_{i,n} = 1 \qquad \qquad i = 1 \cdots Q$$

$$\sum_{i=1}^Q q_{i,n} \leq k \qquad \qquad n = 1 \cdots N$$

$$\text{CNOT}_{i,j} \leq \sum_{n=1}^N |q_{i,n} - q_{j,n}|$$

 $q_{i,n}$ represents a one-hot style encoding of mapping qubit i to one of N memory blocks, and k is the memory block size. Each binary variable $\text{CNOT}_{i,j}$ represents satisfying a CNOT between qubits i and j, with $w_{i,j}$ denoting the number of such CNOT gates in the whole program.

Inserting Loads and Stores: We insert loads and stores greedily. For each time step in the program, we iterate through all active qubits that time step. If a qubit is not in the surface code, we search for an available surface code qubit. If one is found, a load operation is scheduled. If the found surface code is dirty, meaning it has a qubit from a previous time

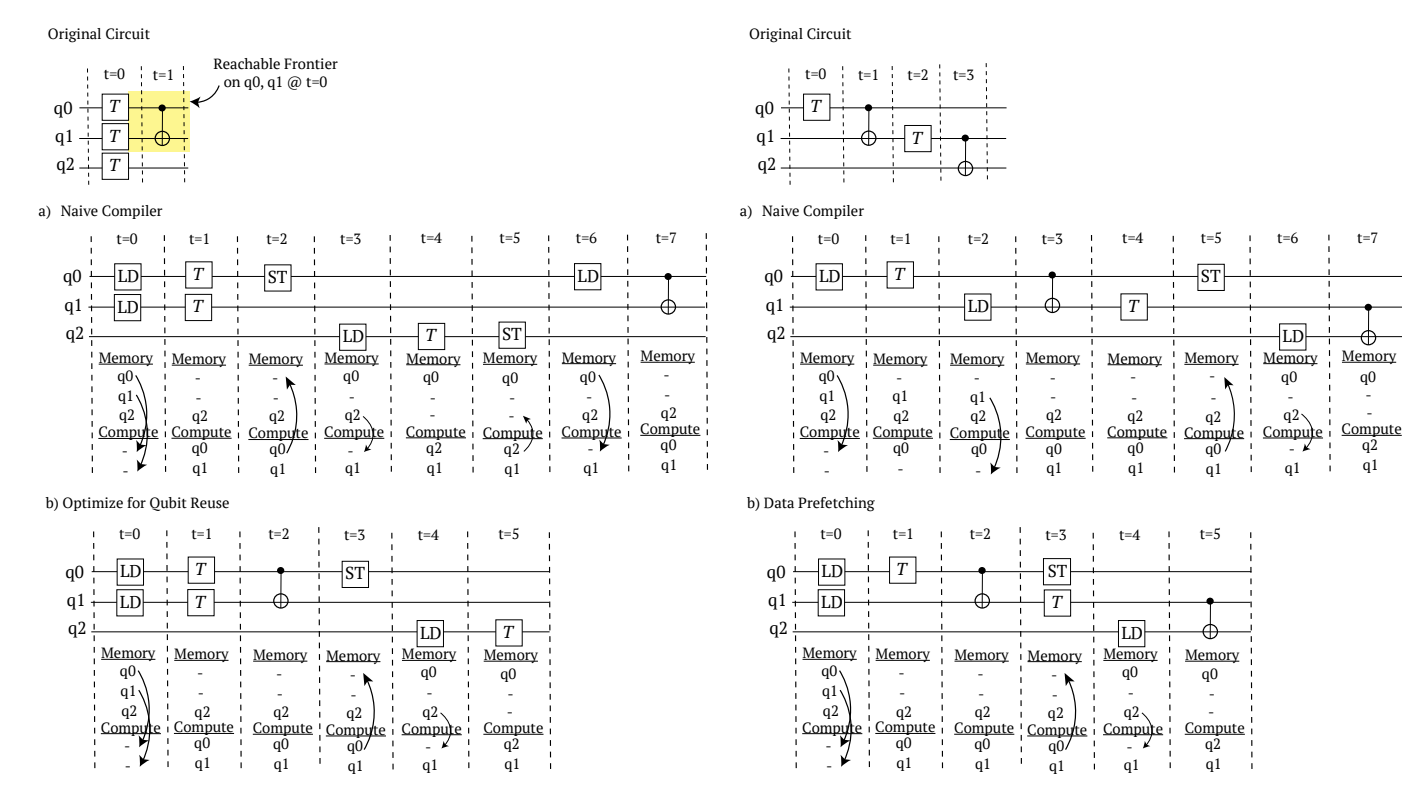


Fig. 9. An example of optimizing for qubit reuse. We can imagine this is a subcircuit of a larger program where qubits q0, q1, and q2 are mapped to separate memory blocks. In a) the naive compiler fully completes each time step in the original circuit before the next. In b) when q2 cannot be loaded, instead of kicking out q0, the compiler reuses q0 and q1 as much as possible without breaking data dependencies before trying to load q2.

Fig. 10. An example of data prefetching. We can imagine this is a subcircuit of a larger program where qubits q0, q1, and q2 are mapped to separate memory blocks. In a) the naive compiler only considers one time step at a time and inserts load operations right before qubits are needed. In b) if there is extra space in compute, the compiler looks ahead for qubits that will be used in the future and loads them in advance.

step, a store operation on the old qubit is scheduled before the load of the active qubit. If no surface code is available, the operation on that qubit is postponed a time step. Finally, if multiple loads and stores occur on the same memory block, they are serialized.

Routing Operations: The compiler needs to route two types of gates in the surface code: CNOT and T. Routing is done greedily each time step. For CNOT gates, a path of ancilla in the routing space is allocated between the two qubits, and for T gates, a single routing ancilla between the data and the resource state factories is allocated. If routing space cannot be allocated for an operation, the operation is delayed a time step.

D. Compiler Optimizations

The compilation methodology described Section VII-C does not include any optimizations. Given that the logical cycle times for loads and stores are twice as long as for compute, minimizing the impact of loads and stores is critical for good program performance in the mixed architecture. In this subsection we describe two compiler optimizations that can be included to address this.

Qubit Reuse: To ensure program correctness, the naive compiler completes all operations in a single time step before the next time step, even if operations are delayed due to

insufficient compute space. For a lot of quantum programs of interest, however, an active qubit may be active the next time step, which we define as **qubit reuse**. So long as the future gates do not break data dependencies, we can keep reusing the active qubits in the surface code, minimizing memory operations.

To address subsets of qubits that exhibit qubit reuse, we modify the compiler's load/store scheduler. When faced with a delayed qubit, meaning all surface codes are already occupied with active qubits, instead of delaying one time step we first calculate the reachable frontier from all qubits currently in the surface code. This captures how many time steps into the future the subset of qubits in the surface code can be reused without breaking data dependencies. The delayed qubit is then postponed to the earliest end frontier. The result is the qubits in the surface code are reused as much as possible before being stored back into memory blocks. An example of this optimization is shown in Figure 9.

Data Prefetching: In the naive compiler, only one time step is considered at a time and LD/STs are inserted right before qubits are needed. If not all surface codes are occupied, we can schedule LD/STs for future qubits in advance, including while gates are occurring. By pre-loading a qubit that will be used in a future time step, we can hide or reduce the miss penalty of the load operation. In classical memory hierarchies, this

Benchmark Name	Abbr.	Appl.	Circuit Width	Average Parallelism	Average Qubit Reuse	Circuit Depth
Quantum Adder [26]	Adder	fact	28, 64, 118, 433	2.8, 3.4, 3.6, 3.8	2.1, 2.6, 2.7, 2.9	305, 597, 1035, 3590
Berstein-Vazarani [6], [26]	BV	algo	30, 70, 140, 280	9.7, 13 , 14.2, 14.2	8.1, 10.8, 11.6, 11.6	25, 43, 79, 159
Quantum Counterfeit Coin [26], [55]	CC	algo	32, 64, 151	8.1, 9.3, 10.2	6, 6.9, 7.5	43, 75, 162
GHZ State Synthesis [26]	GHZ	comm	40, 78, 127, 255	2.8, 2.9, 2.9, 3	1.9, 2, 2, 2	42, 80, 129, 257
Hubbard Prepare Oracle [2], [14]	Hb. Prep.	comm	40, 90, 100	4.4, 4.6, 4.6	3.6, 3.7, 3.7	370, 688, 998
Hubbard Select Oracle [2], [14]	Hb. Sel.	chem	37, 76, 100, 162	2.4, 2.3, 2.3, 2.3	1.9, 1.8, 1.8, 1.8	576, 1284, 2221, 3454
Multiple-Control-Toffoli [14], [32]	MCX	fact	30, 48, 120, 240	2.4, 2.4, 2.4, 2.4	1.9, 1.9, 1.9, 1.9	257, 419, 1067, 2147
Quantum Read Only Memory [2], [14]	QROM	chem	22, 52, 72, 115	2.2, 2.2, 2.1, 2.2	1.7, 1.7, 1.7, 1.7	350, 1434, 3591, 6421
W State Synthesis [26]	W State	comm	36	2.7	2	144

TABLE III
HIGH-LEVEL DESCRIPTIONS OF THE BENCHMARK CIRCUITS SELECTED

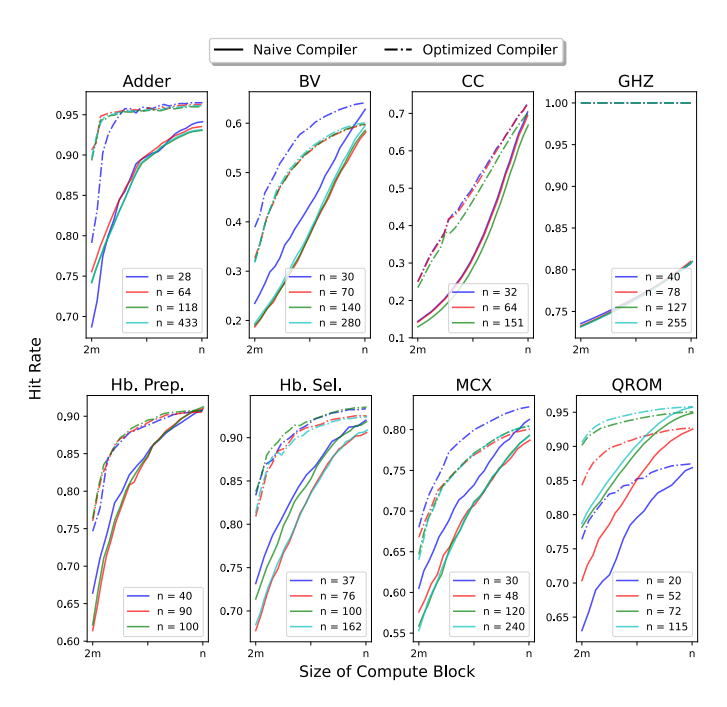


Fig. 11. Hit rates in the mixed architecture for the benchmark circuits we consider with varying number of surface codes in compute. Each time a qubit is used, if it is already in compute the use is deemed a hit, otherwise it is deemed a miss. The hit rate is the # of hits / the total # of uses. Higher is better

technique is known as **prefetching**. To include prefetching, we modify the compiler so that if extra surface codes are available at a given time, we load additional qubits, with a qubit's priority determined by the time until it is next used.

E. Benchmark Programs

To evaluate the performance of our compiler optimizations and compare the two architectures proposed, we choose a suite of available benchmark circuits that have diverse program features and applications, as summarized in Table III. The main sources of benchmark circuits come from open-source repositories qasmBench [26] and Cirq-ft [14].

We identify four main areas of benchmark applications: factoring subroutines (fact.), chemistry simulation subroutines (chem.), resource state for quantum communication and the study of entanglement (comm.), and algorithms that demonstrate complexity theoretic quantum advantage (algo.). Fur-

thermore, we compute basic program features such as average parallelism (the average number of qubits participating in computations of each layer) average qubit reuse (the average number of overlapping qubits across layers), and the depth of the circuit on the baseline architecture.

F. Results and Discussions

In this section, we summarize the performance results of the benchmark programs on the mixed architecture and a baseline surface code only architecture. We report the surface code hit rate and the relative circuit volume in Figure 11 and Figure 12, and the detailed breakdowns of the associated costs in Figure 13 and Figure 14.

As previously noted, the mixed architecture suffers a punishment in circuit execution time (in the form of extra LD/ST operations) when a qubit to be operated on is not in compute. This cost can be defined as the **miss penalty**. By optimizing the access schedule through qubit reuse and qubit prefetching, we can improve the hit rate of our program substantially. From Figure 11 we see a steep gain in hit rate when initially increasing the size of the compute block that eventually plateaus. This gives interesting insight into program structure, and we'd expect it to correlate to the optimal number of surface codes for a given program. Looking at Figure 12, however, for most programs, the extra spatial cost of surface codes does not outweigh the reduced temporal costs from fewer misses, and so the optimal number of surface codes is the fewest possible. Although for some applications, like the Hubbard prepare oracle, we do see the optimal number of surface codes roughly correspond to the plateau of the hit rate.

While qubit reuse and prefetch optimizations can improve hit rate and runtime, they cannot prevent congestion that can occur due to poor mapping of the qubits. The simple ILP mapper we use addresses congestion from CNOTs operating on qubits in the same memory blocks, but does not address congestion from routing many parallel CNOTs in the same routing space. In Figure 13 we observe our ILP mapper does not have a significant impact on the overall compilation performance, suggesting that a more robust mapper that considers routing congestion may be required.

VIII. CONCLUSION

In this work we proposed a novel implementation of a family of qLDPC codes, known as generalized-bicycle codes,

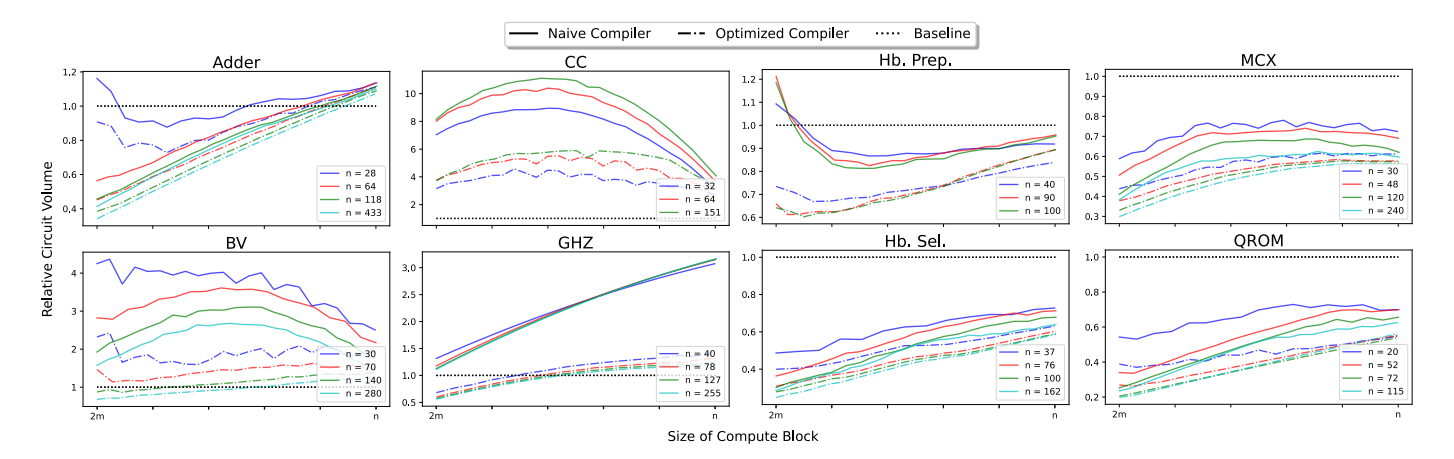


Fig. 12. Circuit volumes in the mixed architecture for the benchmark circuits we consider with a varying number of surface codes in compute. The results are relative to the baseline surface code only architecture. Lower is better.

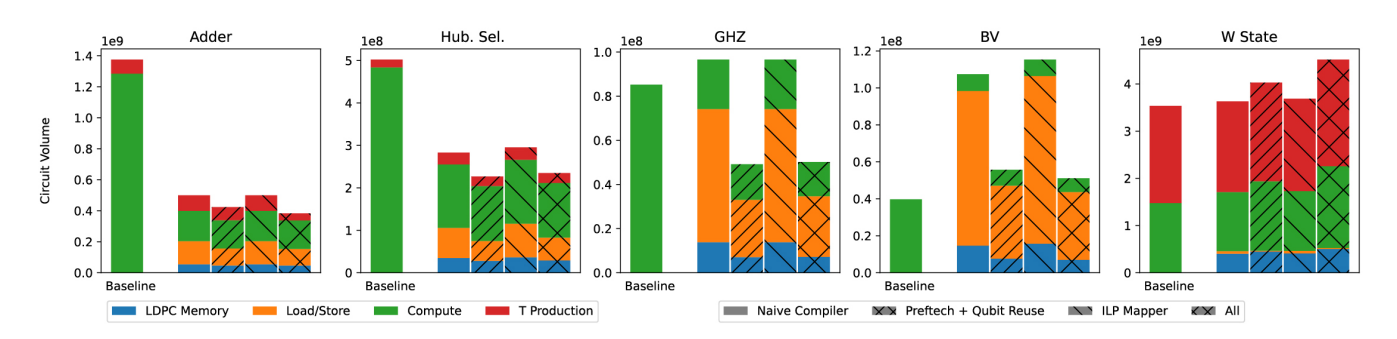


Fig. 13. Bar plots denoting the breakdown of spacetime volume for selected benchmark circuits of average size, ~ 50 qubits. Lower is better. A time step's load/store volume includes the compute space if all compute operations are waiting on loads/stores. This does not change the overall volume, but better highlights the cost of load/store.

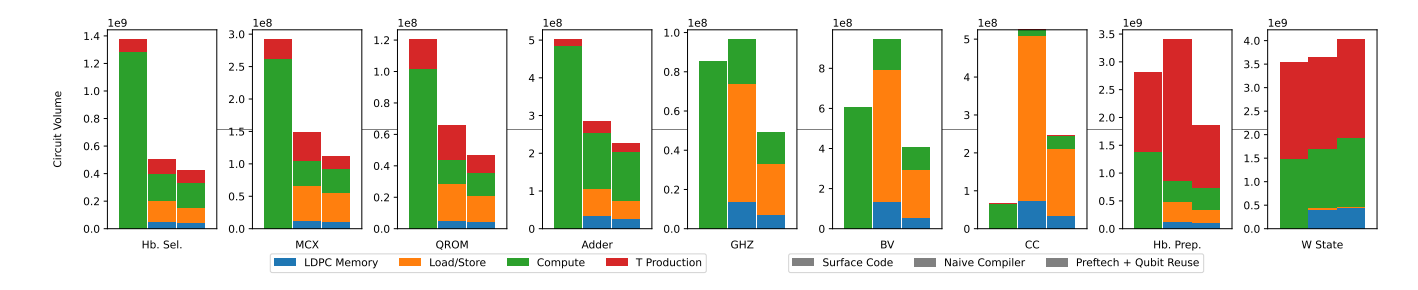


Fig. 14. Bar plots denoting the breakdown of spacetime volume for all benchmark circuits. Lower is better. The circuit size plotted is the one with the largest difference between the naive compiler and the optimized compiler, as seen in Figure 12, to explain where the impact of optimization is.

in atom array quantum computers. We note the repeated check structure inherent in these codes is a good match for the ability to move 2D grids of qubits in atom arrays. For recently discovered codes [10], we find our implementation has comparable logical error rates to the surface code, but with the advantage of the substantially better encoding rates of generalized-bicycle codes, motivating its use as an efficient quantum memory in fault-tolerant systems made from atom arrays.

We also evaluate our implementation's utility as pure mem-

ory. Using a recently proposed model [59], we simulate a mixed architecture of qLDPC memory and surface code compute, leveraging the strengths of both codes. For most programs of interest, the spatial savings from qLDPC memory outweigh the temporal overhead of load and store operations. Furthermore, we note two compiler optimizations: emphasizing qubit reuse and data prefetching, that can have a large impact on the performance of the mixed architecture.

Although our evaluation was performed in the context of atom array quantum computers, we find that many of the conclusions we draw about program structure and compilation for the mixed architecture are broadly applicable to other hardware platforms where separate QEC codes are used for memory and computing. We believe this is a promising model for future fault-tolerant systems with many opportunities for both codesigning QEC with underlying hardware and novel compilation techniques.

IX. ACKNOWLEDGEMENTS

This work is funded in part by EPiQC, an NSF Expedition in Computing, under award CCF-1730449; in part by STAQ under award NSF Phy-1818914; in part by the US Department of Energy Office of Advanced Scientific Computing Research, Accelerated Research for Quantum Computing Program; and in part by the NSF Quantum Leap Challenge Institute for Hybrid Quantum Architectures and Networks (NSF Award 2016136), in part based upon work supported by the U.S. Department of Energy, Office of Science, National Quantum Information Science Research Centers, and in part by the Army Research Office under Grant Number W911NF-23-1-0077. The views and conclusions contained in this document are those of the authors and should not be interpreted as representing the official policies, either expressed or implied, of the U.S. Government. The U.S. Government is authorized to reproduce and distribute reprints for Government purposes notwithstanding any copyright notation herein. FTC is Chief Scientist for Quantum Software at Inflegtion and an advisor to Quantum Circuits, Inc. JL would like to thank Qian Xu and Liang Jiang for discussing qLDPC codes. JL is supported in part by International Business Machines (IBM) Quantum through the Chicago Quantum Exchange, and the Pritzker School of Molecular Engineering at the University of Chicago through AFOSR MURI (FA9550-21-1-0209).

REFERENCES

- [1] J. M. Auger, S. Bergamini, and D. E. Browne, "Blueprint for fault-tolerant quantum computation with rydberg atoms," *Physical Review A*, vol. 96, no. 5, p. 052320, 2017.
- [2] R. Babbush, C. Gidney, D. W. Berry, N. Wiebe, J. McClean, A. Paler, A. Fowler, and H. Neven, "Encoding electronic spectra in quantum circuits with linear t complexity," *Physical Review X*, vol. 8, no. 4, Oct. 2018. [Online]. Available: http://dx.doi.org/10.1103/PhysRevX.8.041015
- [3] J. M. Baker, A. Litteken, C. Duckering, H. Hoffmann, H. Bernien, and F. T. Chong, "Exploiting long-distance interactions and tolerating atom loss in neutral atom quantum architectures," in 2021 ACM/IEEE 48th Annual International Symposium on Computer Architecture (ISCA). IEEE, 2021, pp. 818–831.
- [4] K. Barnes, P. Battaglino, B. J. Bloom, K. Cassella, R. Coxe, N. Crisosto, J. P. King, S. S. Kondov, K. Kotru, S. C. Larsen *et al.*, "Assembly and coherent control of a register of nuclear spin qubits," *Nature Communications*, vol. 13, no. 1, p. 2779, 2022.
- [5] N. Baspin and A. Krishna, "Quantifying nonlocality: How outperforming local quantum codes is expensive," *Physical Review Letters*, vol. 129, no. 5, p. 050505, 2022.
- [6] E. Bernstein and U. Vazirani, "Quantum complexity theory," SIAM Journal on Computing, vol. 26, no. 5, pp. 1411–1473, 1997.
- [7] M. E. Beverland, P. Murali, M. Troyer, K. M. Svore, T. Hoeffler, V. Kliuchnikov, G. H. Low, M. Soeken, A. Sundaram, and A. Vaschillo, "Assessing requirements to scale to practical quantum advantage," arXiv preprint arXiv:2211.07629, 2022.

- [8] D. Bluvstein, H. Levine, G. Semeghini, T. T. Wang, S. Ebadi, M. Kalinowski, A. Keesling, N. Maskara, H. Pichler, M. Greiner et al., "A quantum processor based on coherent transport of entangled atom arrays," *Nature*, vol. 604, no. 7906, pp. 451–456, 2022.
- [9] H. Bombín, "Single-shot fault-tolerant quantum error correction," *Physical Review X*, vol. 5, no. 3, p. 031043, 2015.
- [10] S. Bravyi, A. W. Cross, J. M. Gambetta, D. Maslov, P. Rall, and T. J. Yoder, "High-threshold and low-overhead fault-tolerant quantum memory," arXiv preprint arXiv:2308.07915, 2023.
- [11] S. Bravyi and A. Kitaev, "Universal quantum computation with ideal clifford gates and noisy ancillas," *Physical Review A*, vol. 71, no. 2, p. 022316, 2005.
- [12] A. R. Calderbank and P. W. Shor, "Good quantum error-correcting codes exist," *Physical Review A*, vol. 54, no. 2, p. 1098, 1996.
- [13] L. Z. Cohen, I. H. Kim, S. D. Bartlett, and B. J. Brown, "Low-overhead fault-tolerant quantum computing using long-range connectivity," *Science Advances*, vol. 8, no. 20, p. eabn1717, 2022.
- [14] C. Developers, "Cirq," Jul. 2023. [Online]. Available: https://doi.org/ 10.5281/zenodo.8161252
- [15] Y. Ding and F. T. Chong, "Quantum computer systems: Research for noisy intermediate-scale quantum computers," Synthesis lectures on computer architecture, vol. 15, no. 2, pp. 1–227, 2020.
- [16] S. Ebadi, T. T. Wang, H. Levine, A. Keesling, G. Semeghini, A. Omran, D. Bluvstein, R. Samajdar, H. Pichler, W. W. Ho *et al.*, "Quantum phases of matter on a 256-atom programmable quantum simulator," *Nature*, vol. 595, no. 7866, pp. 227–232, 2021.
- [17] S. J. Evered, D. Bluvstein, M. Kalinowski, S. Ebadi, T. Manovitz, H. Zhou, S. H. Li, A. A. Geim, T. T. Wang, N. Maskara *et al.*, "High-fidelity parallel entangling gates on a neutral atom quantum computer," arXiv preprint arXiv:2304.05420, 2023.
- [18] A. G. Fowler, M. Mariantoni, J. M. Martinis, and A. N. Cleland, "Surface codes: Towards practical large-scale quantum computation," *Physical Review A*, vol. 86, no. 3, p. 032324, 2012.
- [19] J. Ghosh, A. G. Fowler, and M. R. Geller, "Surface code with decoherence: An analysis of three superconducting architectures," *Physical Review A*, vol. 86, no. 6, p. 062318, 2012.
- [20] C. Gidney, "Stim: a fast stabilizer circuit simulator," Quantum, vol. 5, p. 497, 2021.
- [21] T. Graham, L. Phuttitarn, R. Chinnarasu, Y. Song, C. Poole, K. Jooya, J. Scott, A. Scott, P. Eichler, and M. Saffman, "Mid-circuit measurements on a neutral atom quantum processor," arXiv preprint arXiv:2303.10051, 2023.
- [22] D. Horsman, A. G. Fowler, S. Devitt, and R. Van Meter, "Surface code quantum computing by lattice surgery," *New Journal of Physics*, vol. 14, no. 12, p. 123011, 2012.
- [23] A. Jenkins, J. W. Lis, A. Senoo, W. F. McGrew, and A. M. Kaufman, "Ytterbium nuclear-spin qubits in an optical tweezer array," *Physical Review X*, vol. 12, no. 2, p. 021027, 2022.
- [24] A. A. Kovalev and L. P. Pryadko, "Quantum kronecker sum-product low-density parity-check codes with finite rate," *Physical Review A*, vol. 88, no. 1, p. 012311, 2013.
- [25] H. Levine, D. Bluvstein, A. Keesling, T. T. Wang, S. Ebadi, G. Semeghini, A. Omran, M. Greiner, V. Vuletić, and M. D. Lukin, "Dispersive optical systems for scalable raman driving of hyperfine qubits," *Physical Review A*, vol. 105, no. 3, p. 032618, 2022.
- [26] A. Li, S. Stein, S. Krishnamoorthy, and J. Ang, "Qasmbench: A low-level quantum benchmark suite for nisq evaluation and simulation," ACM Transactions on Quantum Computing, vol. 4, no. 2, feb 2023. [Online]. Available: https://doi.org/10.1145/3550488
- [27] H.-K. Lin and L. P. Pryadko, "Quantum two-block group algebra codes," arXiv preprint arXiv:2306.16400, 2023.
- [28] D. Litinski, "A game of surface codes: Large-scale quantum computing with lattice surgery," *Quantum*, vol. 3, p. 128, 2019.
- [29] D. Litinski, "Magic state distillation: Not as costly as you think," Quantum, vol. 3, p. 205, 2019.
- [30] D. Litinski and F. von Oppen, "Lattice surgery with a twist: simplifying clifford gates of surface codes," *Quantum*, vol. 2, p. 62, 2018.
- [31] A. Litteken, J. M. Baker, and F. T. Chong, "Reducing runtime overhead via use-based migration in neutral atom quantum architectures," in 2022 IEEE International Conference on Quantum Computing and Engineering (QCE). IEEE, 2022, pp. 566–576.
- [32] G. H. Low, V. Kliuchnikov, and L. Schaeffer, "Trading t-gates for dirty qubits in state preparation and unitary synthesis," 2018.

- [33] S. Ma, A. P. Burgers, G. Liu, J. Wilson, B. Zhang, and J. D. Thompson, "Universal gate operations on nuclear spin qubits in an optical tweezer array of yb 171 atoms," *Physical Review X*, vol. 12, no. 2, p. 021028, 2022.
- [34] S. Ma, G. Liu, P. Peng, B. Zhang, S. Jandura, J. Claes, A. P. Burgers, G. Pupillo, S. Puri, and J. D. Thompson, "High-fidelity gates with midcircuit erasure conversion in a metastable neutral atom qubit," arXiv preprint arXiv:2305.05493, 2023.
- [35] M. A. Nielsen and I. L. Chuang, "Quantum computation and quantum information," *Phys. Today*, vol. 54, no. 2, p. 60, 2001.
- [36] N. Nottingham, M. A. Perlin, R. White, H. Bernien, F. T. Chong, and J. M. Baker, "Decomposing and routing quantum circuits under constraints for neutral atom architectures," arXiv preprint arXiv:2307.14996, 2023.
- [37] P. Panteleev and G. Kalachev, "Degenerate quantum ldpc codes with good finite length performance," *Quantum*, vol. 5, p. 585, 2021.
- [38] T. Patel, D. Silver, and D. Tiwari, "Geyser: a compilation framework for quantum computing with neutral atoms," in *Proceedings of the 49th Annual International Symposium on Computer Architecture*, 2022, pp. 383–395.
- [39] T. Patel, D. Silver, and D. Tiwari, "Graphine: Enhanced neutral atom quantum computing using application-specific rydberg atom arrangement," in *Proceedings of the International Conference for High Perfor*mance Computing, Networking, Storage and Analysis, 2023, pp. 1–15.
- [40] C. A. Pattison, A. Krishna, and J. Preskill, "Hierarchical memories: Simulating quantum ldpc codes with local gates," arXiv preprint arXiv:2303.04798, 2023.
- [41] H. Poulsen Nautrup, N. Friis, and H. J. Briegel, "Fault-tolerant interface between quantum memories and quantum processors," *Nature commu*nications, vol. 8, no. 1, p. 1321, 2017.
- [42] A. O. Quintavalle, P. Webster, and M. Vasmer, "Partitioning qubits in hypergraph product codes to implement logical gates," *Quantum*, vol. 7, p. 1153, 2023.
- [43] E. G. Rieffel and W. H. Polak, Quantum computing: A gentle introduction. MIT Press, 2011.
- [44] J. Roffe, "Quantum error correction: an introductory guide," Contemporary Physics, vol. 60, no. 3, pp. 226–245, 2019.
- [45] J. Roffe, "LDPC: Python tools for low density parity check codes," 2022. [Online]. Available: https://pypi.org/project/ldpc/
- [46] J. Roffe, D. R. White, S. Burton, and E. Campbell, "Decoding across the quantum low-density parity-check code landscape," *Physical Review Research*, vol. 2, no. 4, Dec 2020. [Online]. Available: http://dx.doi.org/10.1103/PhysRevResearch.2.043423
- [47] N. J. Ross and P. Selinger, "Optimal ancilla-free clifford+ t approximation of z-rotations," arXiv preprint arXiv:1403.2975, 2014.
- [48] M. E. Shea, P. M. Baker, J. A. Joseph, J. Kim, and D. J. Gauthier, "Submillisecond, nondestructive, time-resolved quantum-state readout of a single, trapped neutral atom," *Physical Review A*, vol. 102, no. 5, p. 053101, 2020
- [49] K. Singh, S. Anand, A. Pocklington, J. T. Kemp, and H. Bernien, "Dualelement, two-dimensional atom array with continuous-mode operation," *Physical Review X*, vol. 12, no. 1, p. 011040, 2022.
- [50] L. Skoric, D. E. Browne, K. M. Barnes, N. I. Gillespie, and E. T. Campbell, "Parallel window decoding enables scalable fault tolerant quantum computation," *Nature Communications*, vol. 14, no. 1, p. 7040, 2023.
- [51] B. Tan, D. Bluvstein, M. D. Lukin, and J. Cong, "Qubit mapping for reconfigurable atom arrays," in *Proceedings of the 41st IEEE/ACM International Conference on Computer-Aided Design*, 2022, pp. 1–9.
- [52] D. B. Tan, D. Bluvstein, M. D. Lukin, and J. Cong, "Compiling quantum circuits for dynamically field-programmable neutral atoms array processors," arXiv preprint arXiv:2306.03487, 2023.
- [53] X. Tan, F. Zhang, R. Chao, Y. Shi, and J. Chen, "Scalable surface code decoders with parallelization in time," arXiv preprint arXiv:2209.09219, 2022.
- [54] B. M. Terhal, "Quantum error correction for quantum memories," Reviews of Modern Physics, vol. 87, no. 2, p. 307, 2015.
- [55] B. M. Terhal and J. A. Smolin, "Single quantum querying of a database," *Physical Review A*, vol. 58, no. 3, p. 1822–1826, Sep. 1998. [Online]. Available: http://dx.doi.org/10.1103/PhysRevA.58.1822
- [56] M. A. Tremblay, N. Delfosse, and M. E. Beverland, "Constant-overhead quantum error correction with thin planar connectivity," *Physical Review Letters*, vol. 129, no. 5, p. 050504, 2022.

- [57] J. Viszlai, S. F. Lin, S. Dangwal, J. M. Baker, and F. T. Chong, "An architecture for improved surface code connectivity in neutral atoms," arXiv preprint arXiv:2309.13507, 2023.
- [58] Y. Wu and L. Zhong, "Fusion blossom: Fast mwpm decoders for qec," arXiv preprint arXiv:2305.08307, 2023.
- [59] Q. Xu, J. Ataides, C. A. Pattison, N. Raveendran, D. Bluvstein, J. Wurtz, B. Vasic, M. D. Lukin, L. Jiang, and H. Zhou, "Constant-overhead faulttolerant quantum computation with reconfigurable atom arrays," arXiv preprint arXiv:2308.08648, 2023.
- [60] Y.-C. Zheng, C.-Y. Lai, T. A. Brun, and L.-C. Kwek, "Constant depth fault-tolerant clifford circuits for multi-qubit large block codes," *Quan*tum Science and Technology, vol. 5, no. 4, p. 045007, 2020.